Substrate-Dependent Band Structures in Trilayer Graphene/*h*-BN Heterostructures

Shi Che,[1,*] Petr Stepanov,[1,*] Supeng Ge,[2,*] Menglin Zhu,[3] Dongying Wang,[1] Yongjin Lee,[4] Kevin Myhro,[4] Yanmeng Shi,[4] Ruoyu Chen,[1] Ziqi Pi,[4] Cheng Pan,[4] Bin Cheng,[4] Takashi Taniguchi,[5] Kenji Watanabe,[6] Yafis Barlas,[2,4] Roger K. Lake,[2] Marc Bockrath,[1] Jinwoo Hwang,[3] and Chun Ning Lau[1,4,†]

[1]*Department of Physics, The Ohio State University, Columbus, Ohio 43221, USA*
[2]*Department of Electrical and Computer Engineering, University of California, Riverside, California 92521, USA*
[3]*Department of Materials Science and Engineering, The Ohio State University, Columbus, Ohio 43221, USA*
[4]*Department of Physics and Astronomy, University of California, Riverside, California 92521, USA*
[5]*International Center for Materials Nanoarchitectonics, National Institute for Materials Science, 1-1 Namiki, Tsukuba, Ibaraki 305-0044, Japan*
[6]*Research Center for Functional Materials, National Institute for Materials Science, 1-1 Namiki, Tsukuba, Ibaraki 305-0044, Japan*

(Received 30 April 2018; revised 19 April 2019; accepted 3 November 2020; published 10 December 2020)

The tight-binding model has been spectacularly successful in elucidating the electronic and optical properties of a vast number of materials. Within the tight-binding model, the hopping parameters that determine much of the band structure are often taken as constants. Here, using *ABA*-stacked trilayer graphene as the model system, we show that, contrary to conventional wisdom, the hopping parameters and therefore band structures are not constants, but are systematically variable depending on their relative alignment angle between *h*-BN. Moreover, the addition or removal of the *h*-BN substrate results in an inversion of the K and K' valley in trilayer graphene's lowest Landau level. Our work illustrates the oft-ignored and rather surprising impact of the substrates on band structures of 2D materials.

DOI: 10.1103/PhysRevLett.125.246401

The hopping parameters in the tight-binding model denote the transfer integrals between various atomic sites, and directly govern the band structure of a material, which in turn constitutes the foundation of its electronic, optical, and thermal properties. Conventionally, they are thought to be constants for a given material, and are substrate independent. In fact, with rare exceptions such as strains or superlattice formation induced by close lattice matching, substrates are generally considered "inert," exerting no influence on the band structures of the supported materials. For atomically thin 2D materials, substrates are known to provide screening or host scattering sites, yet their effects on the band structure of the supported material is hitherto not recognized.

Here, we show that, contrary to conventional wisdom, substrates (and the lack thereof) significantly alter the band structure of few-layer graphene. To illustrate the effect of substrates on the band structures of 2D materials, the material under study should be sufficiently thin so that its interaction with substrate is appreciable, but sufficiently complex so as to include entire sets of hopping parameters; moreover, modifications in the band structure should result in discernible features in transport measurements. We choose *ABA*-stacked trilayer graphene (TLG) [1–10], which is the simplest graphite system affording the complete set of tight binding hopping parameters, as a model system to investigate the effect of substrates on band structures. By examining the Landau level (LL) crossing points in TLG that are either suspended or supported on *h*-BN substrates with different alignment angles, we demonstrate that the band structures are not constants, but are systematically modified by the rotation angle between the *h*-BN and TLG sheets, ranging from 0° to 25°. One of the most dramatic manifestations of the effect of substrates is the inversion of K and K' valleys of the lowest Landau level in suspended and *h*-BN–supported devices. The results are supported by DFT simulations that predict increasing graphene/*h*-BN interactions as the two lattices become aligned. Our work underscores the critical role played by substrates in van der Waals heterostructures and offer a route to control and engineer the band structures of 2D materials via substrate engineering.

The band structure of *ABA* TLG can be decomposed into a combination of a monolayer graphene (MLG)-like band and a bilayer graphene (BLG)-like band. Both bands are individually gapped, and vertically offset from each other, with MLG (BLG) band edges at $\delta - \gamma_5/2 + \delta_2$ $(-2\delta_2)$ and $-\gamma_2/2 + \delta_2$ $(\gamma_2/2 + \delta_2)$, respectively, where the γ's are the Slonczewski-Weiss-McClure parameters, δ denotes the energy difference between stacked and unstacked atoms, and δ_2 describes the potential difference between the middle layer and the average of the outer layers. In a magnetic field B, the lowest Landau levels (LLs) for both

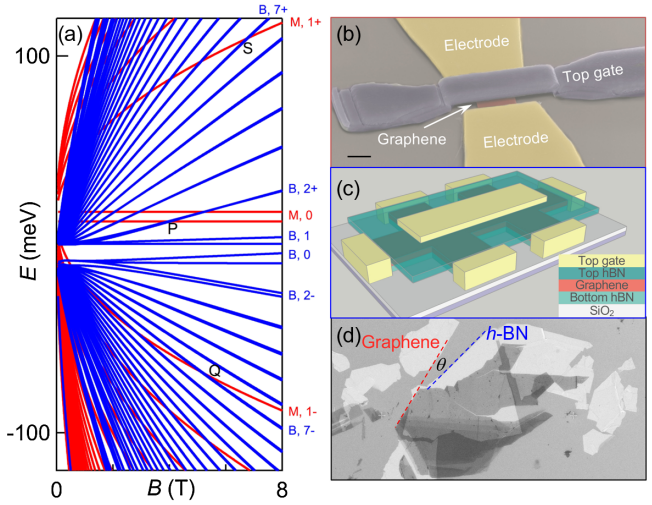

FIG. 1. (a) Typical LL spectra of TLG. Red and blue lines are LLs from MLG- and BLG-like bands, respectively. S, P, and Q indicate LL crossing points. (b) False color SEM image of a dual-gated suspended TLG device. Scale bar: 1 μm. (c) Schematic of the dual-gated h-BN–supported TLG device. Inset: side view of the device schematic. (d) SEM image of a TLG (dark) transferred onto h-BN (bright), the red (blue) dashed line indicates the long, straight edge of TLG (h-BN) used to characterize the twist angle θ.

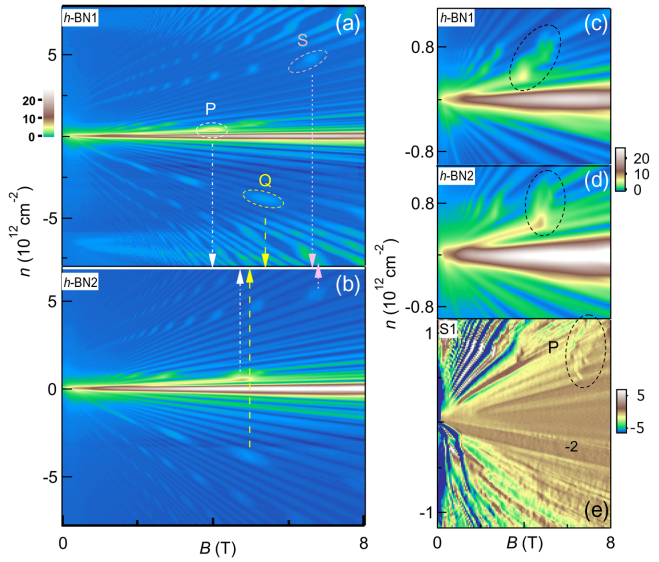

FIG. 2. (a),(b) Landau fan $R_{xx}(n, B)$ at $E_\perp = 0$ for devices h-BN1 and h-BN2, respectively. (c),(d) Low charge density close-up plot of Figs. 2(b) and 2(b), respectively. The color scales in panels (a)–(d) are in kΩ. (e) dG/dB (n, B) fan diagram of suspended device $S1$.

bands, located at the band edges, are almost nondispersive, while the higher $N > 1$ LLs in MLG- and BLG-like bands disperse with $B^{1/2}$ and B, respectively, giving rise to numerous crossing points [Fig. 1(a)]. These LL crossing points are very sensitive to the hopping parameters and are used to extract their values [7,11–15]. However, despite the simplicity of the system and similarity of the techniques, there are considerable variations in the extracted values [7,11–15], sometimes by more than an order of magnitude. Notably, similar discrepancies are found in earlier works on BLG [16–19].

To investigate the impact of substrates on TLG, we fabricate and measure two types of high mobility devices: two-terminal suspended devices [Fig. 1(b)] are fabricated by coupling to Cr/Au electrodes and released from the SiO_2 layer by hydrofluoric acid etching [20–22], while h-BN/TLG heterostructures [Fig. 1(c)] are fabricated by successive sacrificial layer transfers [23,24], SF_6 plasma etching to define Hall-bar geometry and electron beam lithography to pattern electrodes and top gates [25]. For samples supported on h-BN substrates, the twist angle θ between TLG and bottom h-BN is determined by the angle between the long, straight edge of the two types of atomic layers in SEM or optical images [Fig. 1(d)] [25]; these straight edges correspond to an easy-tear direction and are likely to be along the same crystallographic direction [26–32]. Notably, our estimates of θ are confirmed by diffraction studies via transmission electron microscopy of graphene/h-BN stacks [25].

Figures 2(a)–2(c) display longitudinal resistance R_{xx} as a function of charge density n and B at zero out-of-plane electric field $E_\perp$ for two different h-BN–supported devices (h-BN1 and h-BN2) and one suspended device ($S1$). We first examine the Landau fans of the h-BN–supported samples that are fabricated and measured under nominally identical conditions. One of the devices (h-BN1) exhibits secondary Dirac points at $n \sim \pm 6.7 \times 10^{12}$ cm^{-2}, indicating that the presence of a moiré superlattice due to the lattice alignment between TLG flake and the h-BN substrate [33–36]. Apart from this superlattice feature, both Landau fans appear *qualitatively* similar: the dark blue regions, corresponding to vanishing R_{xx} and QH plateaus, fan out from the origin; superimposed on the Landau fans are a series of discrete bright yellow and blue spots that correspond to the crossing points between the LLs that originate from the MLG- and BLG-like bands. For instance, the crossing point that is outlined by the dotted circle P in Fig. 2(a) arises from the crossing between the (M, 0) and the (B, 2) bands, where M and B refer to the MLG- and BLG-like branches, and the numbers indicate orbital LL index, respectively. Similarly, the crossing points Q and S correspond to the intersections of (M, $1-/+$) and (B, $7-/+$) on the hole and electron side, respectively.

Intriguingly, despite being seemingly identical, these two devices display crossing points at different n and B. The most noticeable is crossing point P—it occurs at the $n = 3.6 \times 10^{11}$ cm^{-2} and $B = 4.1$ T for h-BN1, but appears at higher $n = 5 \times 10^{11}$ cm^{-2} and $B = 4.8$ T for h-BN2 [see close-up plots in Figs. 2(c)–2(d)]. Similarly, crossing points Q and S also differ in the two devices—comparing to h-BN1, Q moves to lower B while S to higher magnetic fields in h-BN2. These crossing points that

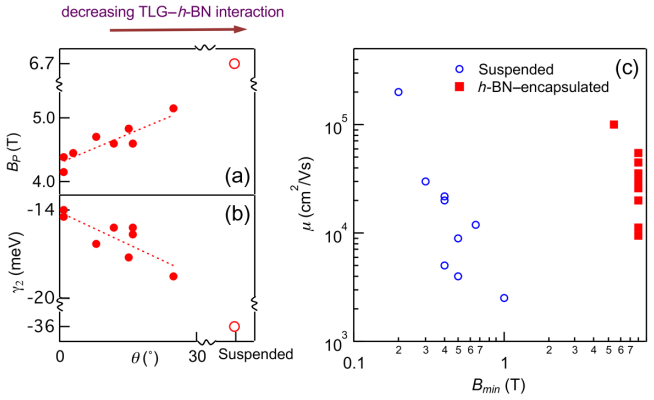

FIG. 3. (a),(b) LL crossing points B_P and extracted hopping parameter γ_2 vs twist angle θ between TLG and h-BN substrate. Data points from a suspended device (hollow symbols) are also shown in the direction of decreasing TLG–h-BN interaction. The dotted lines are linear fits to the data points; however, they are not intended to infer functional dependence on between θ and B_P or γ_2, and should be treated as guides to the eye. (c) Field effect mobility μ of different devices vs the minimum magnetic field B_{min} at which QH state $\nu = -2$ is resolved.

emerge at different values of B in the two devices are indicated by pairwise vertical arrows in Figs. 2(a)–2(b).

The observed variations in LL crossing points in different devices are surprising, and suggest that the hopping parameters, which fully determine the crossing points, are not constants. Such variations cannot arise from the difference in sample mobility, which affects the width (but not location) of the LLs. Inclusion of ABC stacking domains is also extremely unlikely, due to our Raman mapping of the flakes and energetic instability of ABC stacking. Other factors such as strain or charge transfer are also unlikely (see Supplemental Material [25] for a detailed discussion). We therefore explore the possibility that the LL crossing points vary with substrates. To this end, we examine nine different h-BN–supported devices, and plot the crossing points B_P, B_Q, and B_S vs the twist angle θ between the TLG flake and the h-BN substrate [Figs. 3(a) and S3]. As θ decreases, i.e., as h-BN/TLG lattices become aligned, B_Q systematically decreases while B_P increases. Their directions of movement indicate that larger θ shifts the MLG-like bands upward relative to the BLG-like bands, i.e., increases the vertical offset between these two bands, given by $\sim|\gamma_2|$. This is borne out quantitatively by our extraction of γ_2 by fitting the crossing points to calculated LL spectra, which are plotted as blue triangles in Fig. 3(b) (see below for details of the calculation).

These results show that $|\gamma_2|$ increases in samples with small moiré superlattice periods, in which the graphene–h-BN interaction is relatively weak. Following this trend, we achieve the weakest graphene-substrate interaction by removing the substrate altogether. The differentiated two-terminal conductance $dG/dB(n, B)$ of the suspended device $S1$ in Fig. 2(e). Here, the range of n is limited so as to avoid collapsing the suspended membrane under large gate voltages, thus only crossing point P (indicated by the dotted circle) is visible. As expected, it appears at a much higher $B \sim 6.8$ T than that in h-BN–supported devices (similar B_P values are observed in all nine suspended samples). Such large B_P confirms the trend observed in h-BN–supported devices, that is, as the interaction with the substrate weakens, the MLG-like bands moves to higher energies. B_P and γ_2 for $S1$ are plotted as hollow symbols to the right side of Fig. 3(a) on the interrupted x axis in the direction of the decreasing h-BN–TLG interaction.

In addition to the crossing points, another salient difference between $S1$ and h-BN1 emerges as the quantum Hall (QH) state at filling factor $\nu = -2$. Except at very small B, its gap $\Delta_{\nu=-2} \approx |\gamma_2/2 + 3\delta_2|$ arises from the *valley* gap of the lowest LLs in the BLG-like branch, i.e., the energetic separation between (B, K, 0/1) and (B, K', 0/1) levels. Strikingly, this QH state is extremely robust in $S1$ and resolved with quantized conductance at B as small as 0.2 T [Fig. 2(e)]. In contrast, in h-BN–supported devices, it remains unresolved even at 8 T [Figs. 2(c)–2(d)]. To ensure the different $\nu = -2$ stability does not arise from sample-to-sample variations in disorder or contact resistance, we examine eight suspended and nine h-BN–supported devices. The results are summarized in Fig. 3(c), which plots field effect mobility μ vs B_{min}, the minimum B at which the $\nu = -2$ state is resolved. Despite the large range of μ in both types of devices, the resolution of the $\nu = -2$ state is starkly different—it remains unresolved at $B = 8$ T in all but one h-BN–supported device, but is resolved at $B < 1$ T in all suspended devices, including ones with relatively low mobility. Thus, without exception, suspended samples have a significantly larger $\Delta_{\nu=-2}$ than their h-BN–supported counterparts, indicating that the introduction of h-BN substrates significantly modifies the hopping parameters γ_2 and δ_2.

Another piece of evidence emerges in the LL crossings in out-of-plane electric field $E_\perp$. Figure 4(a) displays a data set $R_{xx}(\nu, E_\perp)$ for h-BN1 at $B = 8$ T, where the vertical blue stripes represent incompressible states at integer filling factors with $R_{xx} \sim 0$, interrupted by LL crossings points with high resistance peaks. As $E_\perp$ varies, crossings are observed at all integer plateaus at $\nu > -1$. The observation of crossings at $\nu = -2$ at relatively small $E_\perp \sim \pm 55$ meV is particularly informative: it arises from the crossing of the valley-split lowest LLs of the BLG-like bands. As $E_\perp$ depresses the K' valley while leaves K-valley levels unchanged [10,25], the observed crossing indicate that, at $E_\perp = 0$, the (B, K',0) level has higher energy than (B, K, 1), which is in agreement with a prior study [13]. In suspended samples, however, this crossing is absent [Fig. 4(b)], suggesting that the K-valley LL has higher energy, in agreement with the large $\Delta_{\nu=-2}$ and very high B_P observed for suspended devices.

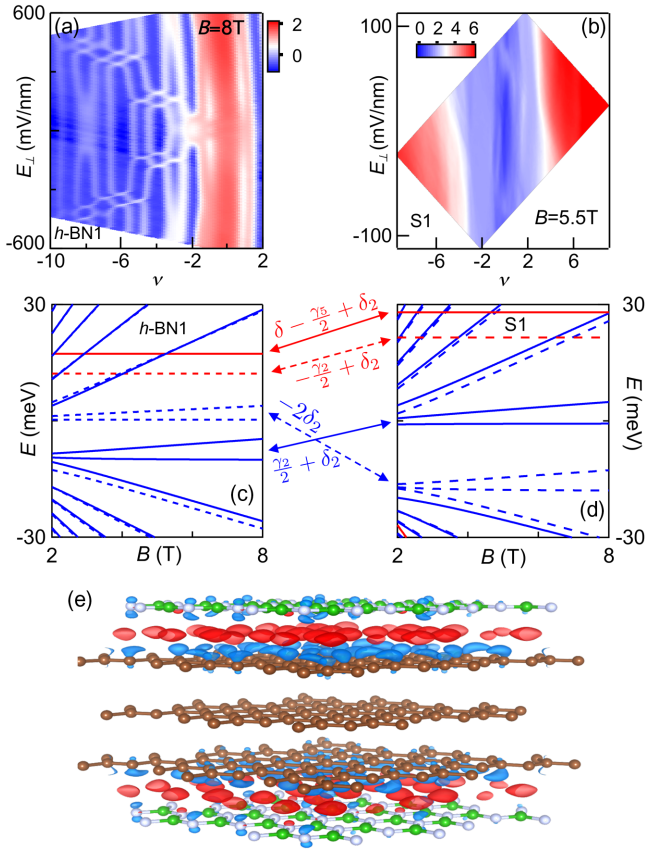

FIG. 4. (a) $R_{xx}(\nu, E_\perp)$ in unit of kΩ at $B = 8$ T of device h-BN1. (b) $G(\nu, E_\perp)$ in unit of e^2/h at $B = 5.5$ T for device $S2$. (c),(d) Calculated low energy LL spectra for device h-BN1 and $S1$, respectively. Red (blue) lines are LLs from MLG-like (BLG-like) band. Solid (dashed) lines address K (K') valley, respectively. The expressions indicate the energies of the lowest LLs in terms of hopping parameters. (e) DFT simulated charge redistribution in h-BN/TLG heterostructure. TLG layers are in brown, h-BN layers are in white and green, the red (blue) isosurfaces denote the charge increase (decrease) regions when adding on h-BN layers.

To quantify the hopping parameters, we fit the experimentally obtained crossing points to the LL spectra calculated by a $k \cdot p$ continuum Hamiltonian [6]. The calculated low energy LL spectrum for devices h-BN1 and $S1$ are shown in Figs. 4(c) and 4(d). (Because of the high degree of sample-to-sample consistency of suspended devices, $S1$ is taken as the generic spectrum of suspended samples.) Thus, the proximity of h-BN substrates not only modifies the hopping parameters, but also causes a "valley inversion" in the lowest Landau level of the BLG-like branch, indicated by the arrows between Figs. 4(c) and 4(d).

The extracted hopping parameters of both devices are summarized in Table I. Here, we adopt an approach of minimal modification—to achieve consistency with data, the minimum set of hopping parameters that need to be adjusted is γ_2 and δ_2. After the introduction of

TABLE I. Hopping parameters in units of meV extracted from experimental data for a suspended and an h-BN–supported TLG device.

Device	γ_0	γ_1	γ_2	γ_3	γ_4	γ_5	δ	δ_2
$S1$	3100	355	−41	315	150	40	47	1
h-BN1	3100	355	−12.8	315	150	40	31.5	5.8

h-BN substrates, γ_2 and δ_2 change by −280% and 560%, respectively. The impact of the h-BN substrate on the band structure is qualitatively understood by a DFT-based simulation. Figure 4(e) illustrates the calculated charge redistribution upon the addition of the h-BN layers, where the blue (red) isosurface represents the region with net charges decrease (increase). We find that partial charges from TLG move toward h-BN, and the wave functions of the top and bottom layers of TLG shift away from each other. Since γ_2 is the coupling between two outer layers of TLG, its magnitude is suppressed with the addition of h-BN; δ_2, which is the difference in energy between the middle layer and the average of the outer layers, increases accordingly. On the other hand, we currently do not have a quantitative model of the band structures' dependence on the twist angle, due to the exceedingly difficult task of simulating very large unit cells with thousands of atoms. Effects of unequivalent carbon atoms with broken lattice symmetries could also be important [34,37]. These detailed considerations will be explored in a future work.

Taken together, our observation indicates that substrates, or the lack thereof, have a much larger impact on the band structure and the LL spectrum than previously thought possible. The set of hopping parameters and the band structure of a given 2D material are not constants, but, like many other parameters in 2D materials, can be modified by different substrates. Such substrate-dependent band structures should be taken into account when interpreting electronic and optoelectronic studies of 2D materials. In the long term, substrate engineering could be employed to tailor the band structures of 2D materials to optimize their applications.

The experiments are supported by DOE BES Division under Grant No. DE-SC0020187. M. Z. and J. H acknowledge support from NSF Materials Research Science and Engineering Centers (MRSEC) DMR-2011876. Electron microscopy was performed at the Center for Electron Microscopy and Analysis at The Ohio State University. Tight binding calculations were supported in part by the NSF EFRI-1433395. K. W. and T. T. acknowledge support from the Elemental Strategy Initiative conducted by the MEXT, Japan, Grant No. JPMXP0112101001, JSPS KAKENHI Grant No. JP20H00354, and the CREST (JPMJCR15F3) JST.

*These authors contributed equally to this work.
†lau.232@osu.edu

[1] B. Partoens and F. M. Peeters, From graphene to graphite: Electronic structure around the K point, Phys. Rev. B **74**, 075404 (2006).
[2] S. Latil and L. Henrard, Charge carriers in few-layer graphene films, Phys. Rev. Lett. **97**, 036803 (2006).
[3] M. Aoki and H. Amawashi, Dependence of band structures on stacking and field in layered graphene, Solid State Commun. **142**, 123 (2007).
[4] M. F. Craciun, S. Russo, M. Yamamoto, J. B. Oostinga, A. F. Morpurgo, and S. Tarucha, Trilayer graphene is a semimetal with a gate-tunable band overlap, Nat. Nanotechnol. **4**, 383 (2009).
[5] W. Z. Bao, Z. Zhao, H. Zhang, G. Liu, P. Kratz, L. Jing, J.Velasco, Jr., D. Smirnov, and C. N. Lau, Magnetoconductance oscillations and evidence for fractional quantum Hall states in suspended bilayer and trilayer graphene, Phys. Rev. Lett. **105**, 246601 (2010).
[6] M. Koshino and E. McCann, Landau level spectra and the quantum Hall effect of multilayer graphene, Phys. Rev. B **83**, 165443 (2011).
[7] T. Taychatanapat, K. Watanabe, T. Taniguchi, and P. Jarillo-Herrero, Quantum Hall effect and Landau level crossing of Dirac fermions in trilayer graphene, Nat. Phys. **7**, 621 (2011).
[8] E. A. Henriksen, D. Nandi, and J. P. Eisenstein, Quantum Hall Effect and Semimetallic Behavior of Dual-Gated ABA-Stacked Trilayer Graphene, Phys. Rev. X **2**, 011004 (2012).
[9] Y. Lee, J. Velasco, D. Tran, F. Zhang, W. Bao, L. Jing, K. Myhro, D. Smirnov, and C. Ning Lau, Broken symmetry quantum Hall states in dual-gated ABA trilayer grapehene, Nano Lett. **13**, 1627 (2013).
[10] M. Serbyn and D. A. Abanin, New Dirac points and multiple Landau level crossings in biased trilayer graphene, Phys. Rev. B **87**, 115422 (2013).
[11] P. Stepanov, Y. Barlas, T. Espiritu, S. Che, K. Watanabe, T. Taniguchi, D. Smirnov, and C. N. Lau, Tunable Symmetries of Integer and Fractional Quantum Hall Phases in Heterostructures with Multiple Dirac Bands, Phys. Rev. Lett. **117**, 076807 (2016).
[12] B. Datta, S. Dey, A. Samanta, H. Agarwal, A. Borah, K. Watanabe, T. Taniguchi, R. Sensarma, and M. M. Deshmukh, Strong electronic interaction and multiple quantum Hall ferromagnetic phases in trilayer graphene, Nat. Commun. **8**, 14518 (2017).
[13] L. C. Campos, T. Taychatanapat, M. Serbyn, K. Surakitbovorn, K. Watanabe, T. Taniguchi, D. A. Abanin, and P. Jarillo-Herrero, Landau Level Splittings, Phase Transitions, and Nonuniform Charge Distribution in Trilayer Graphene, Phys. Rev. Lett. **117**, 066601 (2016).
[14] Y. Asakawa, S. Masubuchi, N. Inoue, S. Morikawa, K. Watanabe, T. Taniguchi, and T. Machida, Intersubband Landau Level Couplings Induced by In-Plane Magnetic Fields in Trilayer Graphene, Phys. Rev. Lett. **119**, 186802 (2017).
[15] Y. Shimazaki *et al.*, Landau level evolution driven by band hybridization in mirror symmetry broken ABA-stacked trilayer graphene, arXiv:1611.02395.
[16] L. M. Malard, J. Nilsson, D. C. Elias, J. C. Brant, F. Plentz, E. S. Alves, A. H. Castro Neto, and M. A. Pimenta, Probing the electronic structure of bilayer graphene by Raman scattering, Phys. Rev. B **76**, 201401(R) (2007).
[17] L. M. Zhang, Z. Q. Li, D. N. Basov, M. M. Fogler, Z. Hao, and M. C. Martin, Determination of the electronic structure of bilayer graphene from infrared spectroscopy, Phys. Rev. B **78**, 235408 (2008).
[18] A. B. Kuzmenko, I. Crassee, D. van der Marel, P. Blake, and K. S. Novoselov, Determination of the gate-tunable band gap and tight-binding parameters in bilayer graphene using infrared spectroscopy, Phys. Rev. B **80**, 165406 (2009).
[19] J. Jung and A. H. MacDonald, Accurate tight-binding models for the π bands of bilayer graphene, Phys. Rev. B **89**, 035405 (2014).
[20] G. Liu, J. Velasco, W. Bao, and C. Ning Lau, Fabrication of graphene p-n-p junctions with contactless top gates, Appl. Phys. Lett. **92**, 203103 (2008).
[21] V. Jairo, Jr, G. Liu, W. Bao, and C. Ning Lau, Electrical transport in high-quality graphene pnp junctions, New J. Phys. **11**, 095008 (2009).
[22] J. Velasco, Jr *et al.*, Transport spectroscopy of symmetry-broken insulating states in bilayer graphene, Nat. Nanotechnol. **7**, 156 (2012).
[23] P. J. Zomer, S. P. Dash, N. Tombros, and B. J. van Wees, A transfer technique for high mobility graphene devices on commercially available hexagonal boron nitride, Appl. Phys. Lett. **99**, 232104 (2011).
[24] C. Pan, Y. Wu, B. Cheng, S. Che, T. Taniguchi, K. Watanabe, C. N. Lau, and M. Bockrath, Layer polarizability and easy-axis quantum hall ferromagnetism in bilayer graphene, Nano Lett. **17**, 3416 (2017).
[25] See Supplemental Material at http://link.aps.org/supplemental/10.1103/PhysRevLett.125.246401 for description of device fabrication, twist angle determination, additional transport data, and calculations of Landau level spectra.
[26] D. Sen, K. S. Novoselov, P. M. Reis, and M. J. Buehler, Tearing graphene sheets from adhesive substrates produces tapered nanoribbons, Small **6**, 1108 (2010).
[27] T. Kawai, S. Okada, Y. Miyamoto, and H. Hiura, Self-redirection of tearing edges in graphene: Tight-binding molecular dynamics simulations, Phys. Rev. B **80**, 033401 (2009).
[28] K. Kim, V. I. Artyukhov, W. Regan, Y. Liu, M. F. Crommie, B. I. Yakobson, and A. Zettl, Ripping graphene: Preferred directions, Nano Lett. **12**, 293 (2012).
[29] X. Huang, H. Yang, A. C. T. van Duin, K. Jimmy Hsia, and S. Zhang, Chemomechanics control of tearing paths in graphene, Phys. Rev. B **85**, 195453 (2012).
[30] A. Yamanaka and S. Okada, Energetics and electronic structure of h-BN nanoflakes, Sci. Rep. **6**, 30653 (2016).
[31] R. Mukherjee and S. Bhowmick, Edge stabilities of hexagonal boron nitride nanoribbons: A first-principles study, J. Chem. Theory Comput. **7**, 720 (2011).
[32] B. Huang, H. Lee, B.-L. Gu, F. Liu, and W. Duan, Edge stability of boron nitride nanoribbons and its application in designing hybrid BNC structures, Nano Res. **5**, 62 (2012).

[33] P. Wang, B. Cheng, O. Martynov, T. Miao, L. Jing, T. Taniguchi, K. Watanabe, V. Aji, C. N. Lau, and M. Bockrath, Topological winding number change and broken inversion symmetry in a Hofstadter's butterfly, Nano Lett. **15**, 6395 (2015).

[34] B. Hunt *et al.*, Massive Dirac fermions and Hofstadter butterfly in a van der Waals heterostructure, Science **340**, 1427 (2013).

[35] L. A. Ponomarenko *et al.*, Cloning of Dirac fermions in graphene superlattices, Nature (London) **497**, 594 (2013).

[36] C. R. Dean *et al.*, Hofstadter's butterfly and the fractal quantum Hall effect in moiré superlattices, Nature (London) **497**, 598 (2013).

[37] J. Jung, E. Laksono, A. M. DaSilva, A. H. MacDonald, M. Mucha-Kruczyński, and S. Adam, Moiré band model and band gaps of graphene on hexagonal boron nitride, Phys. Rev. B **96**, 085442 (2017).